Cerebral Cortex, August 2016;26: 3655–3668

doi:10.1093/cercor/bhw166
Advance Access Publication Date: 9 June 2016
Original Article

ORIGINAL ARTICLE

From Neuron Biophysics to Orientation Selectivity in Electrically Coupled Networks of Neocortical L2/3 Large Basket Cells

Oren Amsalem[1], Werner Van Geit[3], Eilif Muller[3], Henry Markram[3] and Idan Segev[1,2]

[1]Department of Neurobiology, [2]Edmond and Lily Safra Center for Brain Sciences, The Hebrew University, 9190401 Jerusalem, Israel and [3]Blue Brain Project, École polytechnique fédérale de Lausanne (EPFL) Biotech Campus, 1202 Geneva, Switzerland

Address correspondence to Idan Segev, Department of Neurobiology, The Hebrew University of Jerusalem, Edmond J. Safra Campus, Givat Ram, Jerusalem, 9190401, Israel. Email: idan@lobster.ls.huji.ac.il.

Abstract

In the neocortex, inhibitory interneurons of the same subtype are electrically coupled with each other via dendritic gap junctions (GJs). The impact of multiple GJs on the biophysical properties of interneurons and thus on their input processing is unclear. The present experimentally based theoretical study examined GJs in L2/3 large basket cells (L2/3 LBCs) with 3 goals in mind: (1) To evaluate the errors due to GJs in estimating the cable properties of individual L2/3 LBCs and suggest ways to correct these errors when modeling these cells and the networks they form; (2) to bracket the GJ conductance value (0.05–0.25 nS) and membrane resistivity (10 000–40 000 Ω cm^2) of L2/3 LBCs; these estimates are tightly constrained by in vitro input resistance (131 ± 18.5 MΩ) and the coupling coefficient (1–3.5%) of these cells; and (3) to explore the functional implications of GJs, and show that GJs: (i) dynamically modulate the effective time window for synaptic integration; (ii) improve the axon's capability to encode rapid changes in synaptic inputs; and (iii) reduce the orientation selectivity, linearity index, and phase difference of L2/3 LBCs. Our study provides new insights into the role of GJs and calls for caution when using in vitro measurements for modeling electrically coupled neuronal networks.

Key words: electrical coupling, gap junctions, cortical interneurons, membrane time constant, visual cortex

Introduction

Gap junctions (GJs) are clusters of intercellular membrane channels that electrically couple neurons by creating pores that link their intracellular fluid. GJ channels allow ions and small molecules to pass between neurons, thus creating a direct electric link between the connected cells (Goodenough and Paul 2009). GJs are fairly common in the nervous system; they are typically formed between dendrites [but sometimes also between axons (Schmitz et al. 2001)] and they have been found in many brain regions. Examples include GJs among inferior olivary neurons, which are the only connection between these cells (Devor and Yarom 2002), among inhibitory neurons in the cerebellar molecular layer (Rieubland et al. 2014), and, interestingly, among specific subclasses (e.g., large basket cells, LBCs) of inhibitory interneurons in the neocortex (Galarreta and Hestrin 1999; Gibson et al. 1999; Meyer et al. 2002; Avermann et al. 2012) and the hippocampus (Fukuda and Kosaka 2000; Zhang et al. 2004), as well as

among cells in many other regions such as the retina, the olfactory bulb, and the thalamus. Importantly, GJ conductance (GJc) is modifiable both at long (Mathy et al. 2014) and short time scales (Marandykina et al. 2013; Palacios-Prado et al. 2013). Several studies have attempted to estimate the conductance of GJs and have reported values that ranged from 0.1 to 2.4 nS, resulting in coupling coefficients (CCs) of 1.5–9.4% between pairs of electrically coupled cells (Galarreta and Hestrin 1999, 2002; Gibson et al. 1999, 2005; Amitai et al. 2002; Otsuka and Kawaguchi 2013). In these studies, the GJc was estimated assuming that the connected cells were isopotential, thus neglecting the effect of the dendrites, which can result in an underestimation of the actual GJc (Prinz and Fromherz 2003). A comprehensive review of GJs in the brain can be found in a recent volume by Dere et al. (2012).

Because GJs act as fast channels for electrical communication, their putative functions have been explored primarily with respect to the synchronization of network activity (Tamás et al. 2000; Traub et al. 2001; Buhl et al. 2003; Simon et al. 2005; Hu and Agmon 2015). Findings indicate that the capability of GJs to promote synchrony in networks of inhibitory neurons depends on the dendritic location and conductance value of the GJs (Saraga et al. 2006; Pfeuty et al. 2007), the cell's firing frequency (Chow and Kopell 2000; Lewis and Rinzel 2003), and the cell's intrinsic properties (Pfeuty et al. 2003; Saraga et al. 2006). GJs were also shown to be responsible for synchronizing subthreshold voltage oscillations in the inferior olive, a nucleus which is considered to serve as a "timekeeper" for cerebellar activity (Manor et al. 1997; Torben-Nielsen et al. 2012). Surprisingly, GJs may have a synchronizing as well as a de-synchronizing effect on the same system (Golgi cells), depending on the external input (Vervaeke et al. 2010) and, under certain conditions, they might have an overall inhibitory effect (Galarreta and Hestrin 2002; Russo et al. 2013). Axons of hippocampal principal cell were shown to be connected via GJs (Schmitz et al. 2001); these GJs were suggested to be responsible for both ripples and fast ripple oscillations in epileptic patients (Traub et al. 2002; Vladimirov et al. 2013; Simon et al. 2014). In his review, Pereda (2014) emphasized that interactions between chemical and electrical synapses might be required for normal brain development and function. Taken together, the above studies suggest that GJs have numerous functions and, in some brain regions, may have opposing effects (Vervaeke et al. 2010; Russo et al. 2013), hence implying that the role of GJs is far from being fully understood (Rash et al. 2013).

The present study aimed to contribute several new insights to this as yet incomplete picture of GJ functions. We studied L2/3 fast spiking (FS) LBCs (L2/3 LBCs) that are known to be intensely connected to each other via GJs (Meyer et al. 2002; Fukuda et al. 2006; Avermann et al. 2012). In the cat, each parvalbumin-positive (PV^+) L2/3 LBC forms 60.3 ± 12.2 dendritic GJs with other cells [with about 2 GJs per connection; i.e., each cell is connected to 30 ± 6 other similar cells (Fukuda et al. 2006)]. In the molecular layer of the cerebellar cortex of the rat, it was estimated that each basket cell is connected to ~4 other cells, and that each stellate cell is connected to ~1 other cell (Alcami and Marty 2013). It was also shown experimentally that the steady-state CC between electrically coupled L2/3 LBCs in mice ranges from 1.5% to 3.5% (Meyer et al. 2002; Avermann et al. 2012).

We start with a systematic analysis of the effect of GJs on the cable properties of L2/3 LBCs, and show that the additional paths for current sink due to GJs significantly distort the fundamental cable properties of these cells [e.g., the input resistance and the membrane time constant (Rall 1959, 1969, 1977)]. We next propose an approach to obtain a correct estimate of the cable properties of neurons that are embedded in an electrically coupled network, and demonstrate that it is essential to obtain the correct cable parameters for the isolated cell model (without GJs) both to estimate the GJc in L2/3 LBC networks (constrained by in vitro experiments) and to construct a faithful network model formed by these cells. Creating such a model enabled us to analyze the functional impact of GJs on the cells' capability to integrate synaptic inputs, their capability to track fast input fluctuations via the axonal spikes, and the processing of visual-like input in electrically coupled networks. The findings indicate that GJs reduce (broaden) the selectivity of L2/3 LBC interneurons, consistent with the broad selectivity of cortical interneurons observed experimentally, for example, in the auditory cortex (Li et al. 2015) and in the visual cortex (Kerlin et al. 2010; Ma et al. 2010). Furthermore, GJs decrease the linearity index of electrically coupled neurons, which agrees with the low linearity index that was observed experimentally in inhibitory neurons (Niell and Stryker 2008). Finally, we show that GJs reduce the phase difference between L2/3 LBCs. This work thus constitutes a systematic exploration of the impact of dendritic GJs on the cable properties of neurons, and the functional impact of GJs on the processing of sensory inputs.

Materials and Methods

Cable Properties

We used Rall's cable theory (Rall 1959, 1969) to characterize the cable properties of the modeled neuron and the cylindrical neuron models in Supplementary Figures 6–8. In passive cables, the voltage decay following a brief current input can be expressed as an infinite sum of exponential terms:

$$V_m(x,\ t) = B_0 e^{-t/\tau_0} + B_1 e^{-t/\tau_1} + B_2 e^{-t/\tau_2} + B_3 e^{-t/\tau_3} + \cdots$$

Where the B's depend both on the initial conditions and on x, the τ's are the equalizing time constants that describe the flow of current between the different compartments of the cable (this current flow reduces the voltage difference in the cable). For cables with sealed ends, the slowest time constant τ_0 equals the membrane time constant, $\tau_0 = \tau_m = C_m R_m$, where R_m is the specific membrane resistance ($\Omega\,cm^2$) and C_m is the specific membrane capacitance ($\mu F/cm^2$). Theoretically, it is possible to extract τ_0 and τ_1 by "peeling" the voltage transient following a brief current injection to the cell (Rall 1969). The electrotonic length, L, was then calculated in Supplementary Figure 6 as follows:

$$L = \frac{\pi}{\sqrt{\tau_0/\tau_1 - 1}}.$$

NEURON Simulations

Simulations were performed using the NEURON simulator (Carnevale and Hines 2006) running both on local clusters (NEURON 7.3) and on a supercomputer (NEURON 7.4). The local clusters are based on 14 Intel Xeon E5-2670 v2 (280 threads in total) and 40 Intel Xeon E5-2670 (640 threads in total). The BlueGen/Q system supercomputer is composed of 4 racks of 1024 nodes, each node is based on an IBM PowerPC A2, 1.6 GHz with 16 cores.

Experimental Database for L2/3 Large Basket Interneurons

The 4 L2/3 interneurons shown in Supplementary Figure 1A were used as the building blocks for constructing the network model in the present study. These were LBCs from P14 of the rat. These cells were reconstructed in 3D and one of these cells (shown in

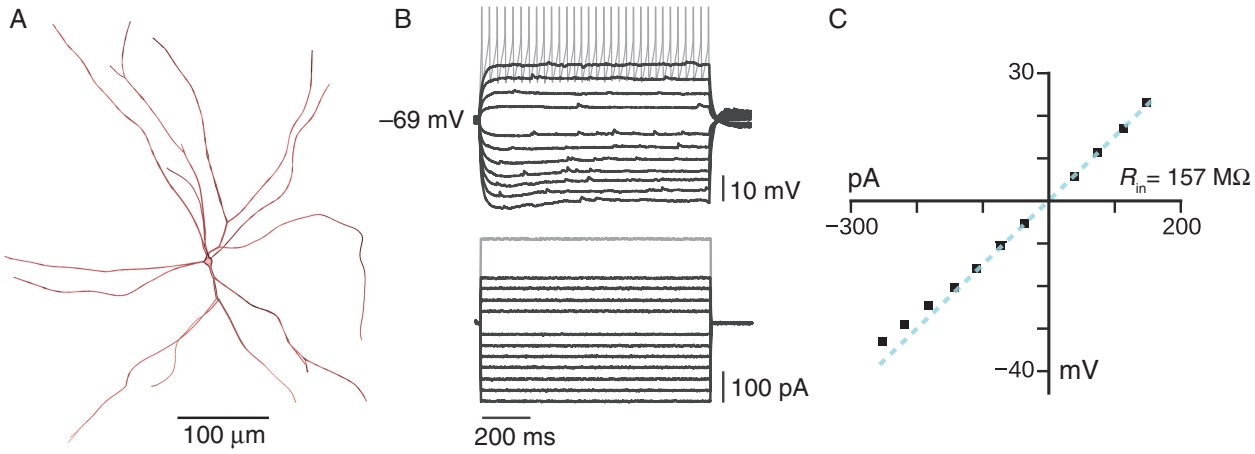

Figure 1. Passive properties of an exemplar L2/3 LBC measured in vitro. (*A*) Three-dimensional reconstructed LBC from L2/3 of the rat. (*B*) Series of hyper- and depolarizing current steps (lower traces) and the corresponding voltage response (upper traces) for the cell shown in *A*. Spikes in gray are truncated. (*C*) *I*/*V* curve (black squares) extracted from *B*; the slope at resting potential yields an input resistance of 157 MΩ. The membrane time constant τ_m for this neuron, estimated from the initial phase of the voltage response to the smallest currents, was 12–15 ms (see Materials and Methods). Three additional L2/3 LBCs used for network modeling are presented in Supplementary Figure 1.

Fig. 1) was also characterized physiologically in vitro [for complete experimental details, see Wang et al. (2002)]. In addition to these 4 reconstructed cells, in vitro electrophysiological recording were made in 6 other L2/3 PV^+ LBC cells; these cells were not morphologically reconstructed; they were classified as FS neurons, with an input resistance of 131 ± 18.5 MΩ, a spike half-width of 1.3 ± 0.25 ms and a firing rate (FR) that reached 59 ± 21 Hz (Meyer et al. 2002; Druckmann et al. 2013). These parameters are somewhat different from those of previously classified FS cells; this difference can be accounted for by the young age (P14) of the animals used (Zhou and Hablitz 1996; Anastasiades et al. 2016).

Building the L2/3 LBC Networks

We ran simulations in networks of 121 neurons (see above); the GJ connectivity between dendrites was random and created as follows. Assume a predefined target connectivity of, for example, 30 ± 6 connections per neurons. Then, (1) Start with the first neuron and form GJs with *n* randomly selected neurons, where *n* is drawn from a normal distribution, with an average of 30 and standard deviation (SD) of 6 [$n \sim N(30,6^2)$]. (2) For the next neuron, select random neurons so that (i) the number of neurons to be connected is drawn from $\sim N(30,6^2)$ minus the number of connections that the cell already has and (ii) select neurons that are not already connected to it and that have fewer than the expected number of connections. We repeated step 2 until the last neuron. This process resulted in some neurons having more than the target connections. Connections between any 2 neurons were realized with a randomly selected number of GJs (1, 2, or 3 GJs per connection with a probability of 0.1, 0.8, or 0.1, respectively). The conductance of each GJ in the network was chosen from a normal distribution with an SD that was 20% from the mean (e.g., 0.4 ± 0.08 nS).

Passive Parameters for L2/3 LBCs

Our goal was to match the distribution of R_{in} in the modeled network to that found in vitro, namely 131 ± 18.5 MΩ (see above). For this purpose, R_m for each modeled cell in the network was selected from a normal distribution with a mean that was dependent on the morphology of the cell (9300 ± 500, 9300 ± 500, 11 400 ± 500, and 11 100 ± 500 Ω cm^2 for C230300D1, C050600B1, C250500A-I4, and C28119A-IN, respectively, see Supplementary Fig. 1*A*), resulting in the R_{in} distribution shown in Supplementary Figure 1*C*, which is in line with the experimental range of R_{in}. Next, for each GJc and depending on the number of connections per cell in the network, the R_m of each cell was adjusted in order to compensate for the current leak due to the GJs, so that the R_{in} of each neuron remains fixed regardless of the GJs. The specific axial resistance (R_a) was set to 100 Ω cm unless stated otherwise and C_m to 1 µF/cm^2. The number of compartments representing the 4 modeled cells was: 167, 169, 231, and 241 for C050660B1, C230300D1, C250500A-I4, and C281155A-IN, respectively.

Incorporation of Active Conductances to Modeled Neuron

We utilized a feature-based multiobjective optimization (MOO) protocol as previously described (Druckmann et al. 2007; Markram et al. 2015) to fit the isolated L2/3 LBC neuron model to in vitro voltage traces. The experimental voltage traces used as a target for the model consisted of 3 different stimulus protocols: (1) Three different subthreshold current injections (–0.22, 0.04, and 0.15 nA) of 1000 ms each. (2) Five repetitions of long (2000 ms) suprathreshold current injections (0.27 nA). (3) Five repetitions of short (45 ms) suprathreshold (0.33 nA) current injections. Basic features (such as input resistance, spike shape, and frequency) were extracted (a full description of the features can be found in Supplementary Material) from the in vitro voltage traces. The mean and SD of each feature were then used as a target for the MOO algorithm.

The free parameters in the optimization were the specific membrane resistivity, the densities of 11 active ion channels, and the dynamics of intracellular Ca^{2+} (Hay et al. 2011). The neuron was separated into different regions: (1) The axon initial segment, (2) the soma, and (3) the dendrites. Each region had a separate set of membrane channels with different conductance densities. The full list of parameters for each region is provided in Supplementary Table 1. R_a and C_m values were not optimized and were set to 100 Ω cm and 1 µF/cm^2, respectively.

The optimization algorithm is explained in detail in Druckmann et al. (2007), Hay et al. (2011), and Markram et al. (2015). In brief, at

the beginning of the algorithm, 1365 models (different parameter sets) were randomly created and the experimental protocols explained above were executed for each of the models. The models with the smallest difference between their voltage trace features and the in vitro features were mutated together and passed to the next generation. The evolutionary algorithm ran on 512 cores of a BlueGene/Q system for 180 generations. For the purpose of this work, we took a model from the last generation.

Tracking of High-Frequency Modulations

To measure the capability of the neuron to track high-frequency modulations, a noisy current $I(t)$ was injected into the soma of a single neuron as described below. The current was composed of 3 components (Fourcaud-Trocme et al. 2003; Köndgen et al. 2008; Tchumatchenko et al. 2011; Ilin et al. 2013):

$$I(t) = I_0 + I_1 \sin(2\pi f t) + I_{noise}$$

where I_0 is the steady-state (DC) current, I_1 the modulated input (as a function of f, frequency), and I_{noise} the noise component which was generated as a realization of an Ornstein–Uhlenbeck stochastic process with zero-mean, variance s^2, and time correlation τ_{noise} = 5 ms (Rauch et al. 2003; Köndgen et al. 2008). For each GJc, s^2 was adjusted to mimic in vivo like membrane fluctuations [voltage SD of 2–5 mV; (Paré et al. 1998)]. I_0 was adjusted to yield a mean FR of approximately 10 Hz (Gentet et al. 2010; Niell and Stryker 2010). The ratio of I_0 to I_1 was 6. In each model, 200 current inputs with different frequencies ranging from 0 to 2000 Hz were used. Each input lasted 30 s using a time-step (dt) of 0.025 ms (in the 0-Hz condition, to obtain a better onset rapidness estimation, dt was set to 0.002 ms). We quantified the ability of a neuron to phase-lock to the fluctuating input by using a method based on the Fourier transform (Tchumatchenko et al. 2011; Eyal et al. 2014). For each frequency, we computed the vector strength $r(f) = \mathrm{abs}(\sum_{j=1}^{N} \exp(i2\pi f t_j))/N$. t_j is defined as the phase shift of each spike in relation to the frequency period (Tchumatchenko et al. 2011; Eyal et al. 2014). To determine the statistical significance of the phase-locking, for each frequency, we used the mean FR of the resulting spike train to create 1500 Poisson spike trains with the same FR, and computed r for each generated spike train. This resulted in a population of r values (r_s). We then calculated the 95th percentile of r_s, that is, the value above 95% of the r's in the population. The probability of obtaining a value above the 95th percentile by chance is 5%. (These values are shown in Fig. 6D as significance levels.) The tracking capability of a model was defined as the frequency that resulted in a spike train with an r value that was lower than the corresponding 95th percentile. To compare different models and inputs, the strength R (Fig. 6) was normalized to the reference value of r at 12 Hz: $R(f) = r(f)/r(12\ \mathrm{Hz})$.

The speed of the action potential (AP) onset was quantified using onset rapidness (Naundorf et al. 2006) defined as the slope of the phase plot at $dV/dt = 5\ \mathrm{mV\ ms^{-1}}$.

In all the "high-frequency tracking" simulations (Fig. 6), R_m values were set to those which yielded an average of 2.5% CC between the modeled cells (Fig. 2; see Supplementary Fig. 5A), the simulations were performed in networks of 121 neurons, and each neuron was connected to 30 ± 6 other neurons with a mean of 2 GJs per connection.

Simulation of Orientation Selective Visual Input

The simulation of a visual input (Fig. 7) consisted of 9 trials; each trial simulated the response of the cell to a different visual orientation θ_{orient}, out of a set of 9 orientations (θ_{orient} = 0°–160°, in 20° increments). Each L2/3 LBC model received 50 orientation selective excitatory axons [α-amino-3-hydroxy-5-methyl-4-isoxazolepropionic acid (AMPA) synapses, see below], with 5 synapses per axon. The mean FR of each axon was determined by the difference (in degrees) between the predefined axon's preferred orientation (PO), θ_{axon}, and the orientation of the visual input, θ_{orient} (eq. 1). For each L2/3 LBC in the network, we randomly assigned a PO; the PO of its input axons was drawn from a normal distribution with a mean that matched the PO of that cell and with a variance of 10°. The axonal ("sensory") input was realized as an inhomogeneous Poisson process with a time-dependent intensity $\lambda(t)$, equation (2), modulated at 2 Hz. For each cell, we randomly selected a phase $(0,2\pi)$ and all the axons impinging a cell had the same phase as the one selected for that particular cell.

The FR of each orientation selective axon was predetermined for each trial according to the axon's PO (θ_{axon}) and the orientation of the visual stimulus (θ_{orient}), as follows:

$$f(\theta_{orient}) = \frac{f_0}{A} \exp\left(\frac{\cos 2(\theta_{orient} - \theta_{axon})}{w}\right) \quad (1)$$

where $A = \frac{1}{\pi}\int_0^{\pi} \exp(\cos(\theta)/w)\mathrm{d}\theta$ is a factor that sets the mean FR to f_0, f_0 was set to 2.5 Hz, and the parameter w determines that the width of the tuning curve, w, was set to 1.

The intensity of the inhomogeneous Poisson process was set as follows:

$$\lambda(t) = f(\theta_{orient}) \times \frac{(\sin((t + \mathrm{phase}) \times f \times 2\pi) + 1)^{1.5}}{B} \quad (2)$$

where t is time in seconds, phase the input phase, f the frequency which was set to 2 Hz, and $B = \int_0^1 \sin(t \times 2\pi)^{1.5}\mathrm{d}t$ is a normalization factor, so that the mean FR would be equal to $f(\theta_{orient})$.

In addition to the orientation selective axons, each L2/3 LBC received 200 excitatory axons (5 AMPA synapses per axon; a total of 1000 synapses) and 25 inhibitory axons [10 γ-aminobutyric acid ($GABA_A$) synapses per axon, a total of 250 inhibitory synapses] that were not orientation selective ("background activity"). Namely, their FR was constant in all orientation settings. The rise and decay time constants of the AMPA synapse were 0.3 and 2 ms, respectively (Angulo et al. 1999), and the reversal potential of the synapse was set to 0 mV. $GABA_A$ synapses had rise and decay time constants of 1 and 8 ms, respectively (Xiang et al. 1998; Gupta 2000), and the reversal potential was set to −80 mV. The resting membrane potential of the modeled cell was −80 mV. The unorientated AMPA axons had an average FR of 1.5 Hz (Gentet et al. 2010), and the $GABA_A$ axons had an average fire rate of 10 Hz (Gentet et al. 2010; Niell and Stryker 2010). The maximal $GABA_A$ conductance was set to 0.125 nS, yielding (in an isolated cell) an average somatic inhibitory postsynaptic potential (IPSP) amplitude of −0.5 mV at a holding potential of −70 mV for a single axon (Avermann et al. 2012). For each GJc setting, the conductance of the AMPA synapse was fitted, so that the resulting mean FR of the 121 neurons of the network would be approximately 10 Hz (Gentet et al. 2010; Niell and Stryker 2010). In the AMPA conductance fitting process, all orientation selective axons fired at 2.5 Hz.

The strength of the orientation selectivity index (OSI) was quantified using the following equation:

$$\mathrm{OSI} = \frac{\sqrt{\left(\sum_i R(\theta_{orient}) \times \sin(2\theta_{orient})\right)^2 + \left(\sum_i R(\theta_{orient}) \times \cos(2\theta_{orient})\right)^2}}{\sum_i R(\theta_{orient})}$$

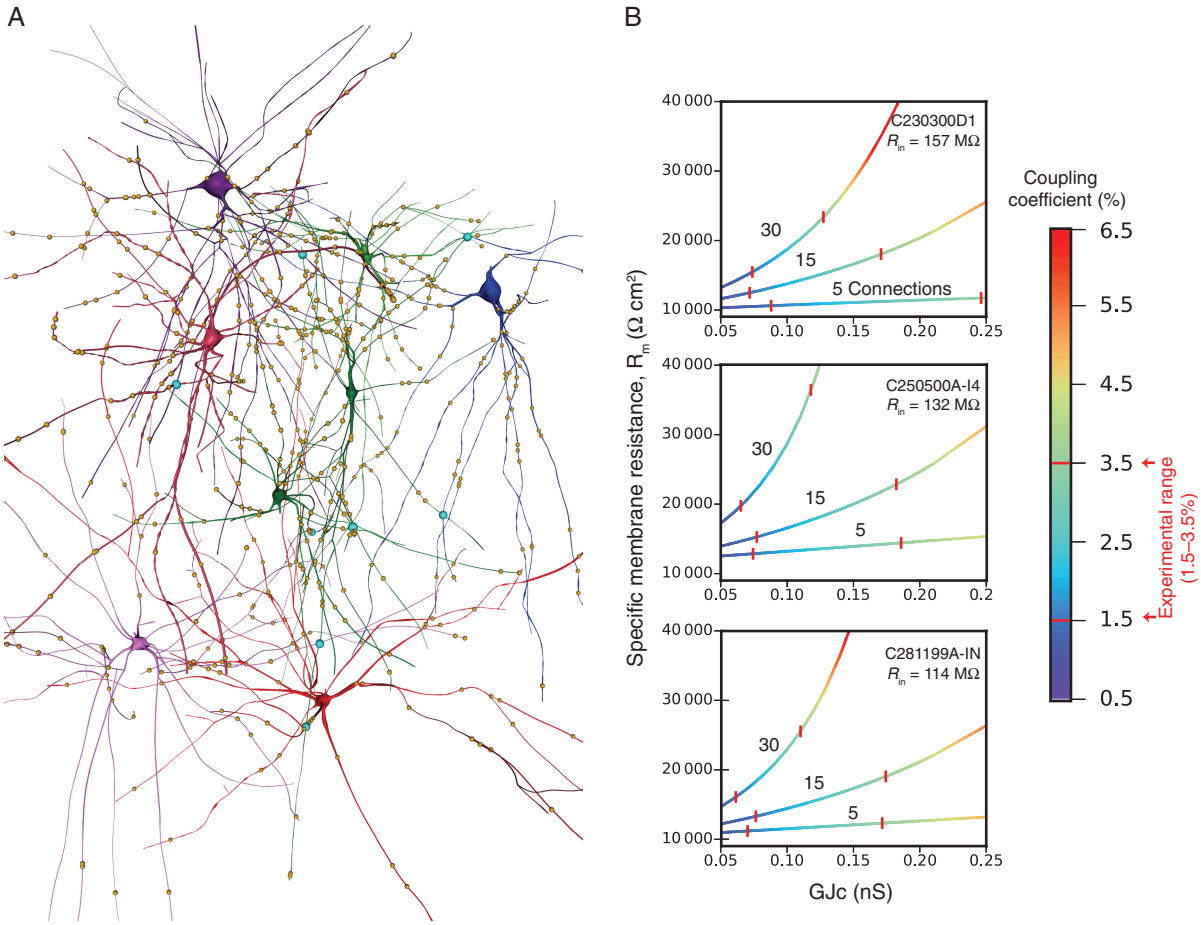

Figure 2. Constraining GJc and R_m values in L2/3 LBCs by fitting the model to the experiments. (*A*) Part of the modeled L2/3 LBC network (blue dots—GJs between these 8 neurons; brown dots—GJs with other neurons which are not shown here). The full network consists of 121 L2/3 LBCs (composed of 4 different morphologies, each with variability in the number of connections/cell, number of contacts/connection, and variability in R_m and in GJc values; see Supplementary Fig. 1 and Materials and Methods). (*B*) Relationship between GJc and the corresponding R_m value consistent with the range of the in vitro values of the experimental R_{in} (ranging from 103 to 157 MΩ; see Materials and Methods). Three exemplar modeled cells (and their corresponding R_{in} values) are shown. In each case, 3 different network configurations (mean number of connections per cell) are shown (see also the corresponding analytical result for the case without dendrites in Supplementary Fig. 2). Color code at right represents the average CC between the modeled cell and its directly connected neighbors; the 2 red arrows at right demarcate the experimental range of the CC (1.5–3.5%); this range is also marked by the 2 vertical lines on each curve. In these 3 examples, and depending on the connectivity level via GJs, R_m was estimated to range from 10 000 to 40 000 Ω cm^2 and GJc from 0.05 to 0.25 nS. The range of R_m and GJc for the whole population is shown in Supplementary Figure 3. The axial resistivity R_a was 100 Ω cm (see Supplementary Fig. 4 for estimates of GJc and R_m with R_a = 200 Ω cm).

where θ_{orient} is the simulated orientation and $R(\theta_{orient})$ the FR of the neuron at this orientation after subtraction of the baseline FR, defined as the neurons' FR when the orientation selective axons are inactive (Ma et al. 2010).

To determine the PO of a cell, we fitted the data with the von Mises function, which is defined as:

$$M(\theta) = A \cdot e^{b[\cos(\theta - c)]}$$

where A is the FR at the PO, c the PO, and b a width parameter (Swindale 1998; Jeyabalaratnam et al. 2013).

The linearity of the response was calculated from the response of the cells to the simulated drifting grating (at the PO of the cell), the output spikes were binned at 100 ms (subtracting the spontaneous FR), and then we applied the discrete Fourier transform and computed F1/F0, the ratio of the first harmonic (response at the drifting frequency, 2 Hz) to the 0th harmonic (mean FR); this ratio was previously used to classify neurons as complex and simple cells (Hochstein and Shapley 1976).

The phase difference between 2 cells was calculated as the difference between the mean phase of their spike timing (Fig. 8C). Only cells that passed the Rayleigh test were considered (Berens 2009).

In the simulation shown in Figures 7 and 8, each cell was connected to 30 ± 6 other cells with a mean of 2 GJs per connection. For each GJc value, we compensated for the decrease in input resistance by increasing R_m (Fig. 2).

Coupling Coefficient

In all cases, the strength of electrical coupling between cells was calculated by injecting a steady current in one cell and recording the resultant voltage in the other cell (Bennett 1977).

Results

Cable Properties and GJ Conductance Obtained via Experimentally Constrained Models

To explore the impact of GJs on the cable properties (input resistance, R_{in}, and membrane time constant, τ_m) of L2/3 LBCs, we first developed detailed compartmental models of 3D reconstructed

and physiologically characterized L2/3 LBCs from the rat neocortex in vitro (see Materials and Methods). We constructed 4 models of four 3D reconstructed L2/3 LBCs as shown in Supplementary Figure 1. One of the modeled cells is shown in Figure 1A, with its 3D morphology reconstructed, its voltage response to current steps (Fig. 1B), and the corresponding steady-state *I*/*V* relationship (Fig. 1C). The input resistance of this cell was 157 MΩ (dashed blue curve in Fig. 1C), and the membrane time constant, obtained by "peeling" (Rall 1969) the rising phase of the smallest hyper- and depolarizing currents in Figure 1B, was estimated to be approximately 12–15 ms (not shown). We stress once again that these are in vitro values; in other words, these measurements were obtained when this neuron (as well as those shown in Supplementary Fig. 1) was embedded in an electrically coupled network. What would the cable properties (R_{in} and τ_m) of these cells be "in isolation", without GJs?

To answer this question, we reconstructed network models of L2/3 LBCs; these modeled cells were electrically connected via GJs (Figs 2A and 3A). The network consisted of 121 L2/3 LBCs composed of a mixture of the four 3D reconstructed cells from young rats shown in Supplementary Figure 1. Each of these morphologies was cloned 30 times, jittering R_m value in the clones, such that the distribution of R_{in} in the whole network is consistent with the experimental variance of R_{in} (see Supplementary Fig. 1C; see Materials and Methods). Information about the number of GJs/neuron is not available for rodents; in the cat, the estimate is that each L2/3 LBC connects to other cells via 60 GJs (Fukuda et al. 2006). In our circuit model, each neuron was connected via GJs to either 5 ± 1 or 15 ± 3 or to 30 ± 6 other neurons (3 different networks) and each connection consisted of 1–3 GJs (see Materials and Methods). Constraining this modeled network by in vitro measurements of both R_{in} (ranging from 105 to 157 MΩ) and CC [ranging, in mice, from 1.5% to 3.5% (Meyer et al. 2002; Avermann et al. 2012)] provided estimates for the values of R_m and GJc that fit these measurements (see below). For the 3 exemplar cells in Figure 2B, R_m ranged from 10 000 to 12 000 Ω cm^2 (for an LBC network with an average of only 5 connections/neuron) to 15 000–40 000 Ω cm^2 (for networks with an average of 30 connections/neuron). The corresponding value for the GJc between L2/3 and L2/3 LBCs ranged from 0.05 to 0.25 nS. The distribution of values for R_m and GJc for the 121 cells composing the whole network is shown in Supplementary Figure 3. This range of values for GJc is smaller than previously used (Traub et al. 2001; Hjorth et al. 2009; O'Connor et al. 2012). This is because these studies did not constrain the modeled network by the experimental R_{in}, as we did in the present study (see Supplementary Fig. 5 for the estimate of GJc when R_{in} is not constrained and Discussion). The corresponding analytical result for the case without dendrites is depicted in Supplementary Figure 2, and demonstrates the strong impact of GJc and the number of GJs on the input resistance of the cell.

Once we had the membrane properties of L2/3 LBCs, we were in a position to estimate the impact of GJs on the cable properties of these cells. For example, taking the case in Figure 2B, top, with a network consisting of an average of 30 connections per cell and a mean GJc = 0.1 nS, the estimated R_m of the cell was approximately 20 000 Ω cm^2. On the basis of this value, the input resistance of this cell, when taken out of the network, was 304 MΩ (compared with 157 MΩ, when it was embedded in the network), and its actual membrane time constant was 20 ms (assuming C_m of 1 μF/cm^2) compared with approximately 10 ms, when it was electrically coupled with the network. To fully explore the distortion due to GJs of the cable properties in L2/3 LBCs and propose ways to correct for this distortion, we next discuss Figure 3.

Distortion of the L2/3 LBC Cable Properties due to GJs and its Correction

Figure 3C1,C2 explores the impact of electrical coupling on the cable parameters ($\tau_{0,peel}$, R_{in}) of L2/3 LBCs. These parameters were computed when the cells were embedded in an electrically coupled network normalized by the corresponding values for the isolated L2/3 LBCs (when GJs = 0 nS). Three sets of network configurations are shown (with 5 + 1, 15 ± 3, or 30 ± 6 connections per cell, each with 1–3 GJs). For each connectivity setting, the isolated cell models were constructed by using the R_m values that corresponded to an average of a 2.5% CC between the modeled cells (Fig. 2; see Supplementary Fig. 5A). Figure 3A, right shows a schematic of the modeled network. Figure 3B1 shows 3 normalized voltage traces (for 3 average values of GJc—0, 0.1, and 0.5 nS, and an average of 30 connections/cell), measured in the middle (red) cell in Figure 3A right, following a brief transient current injected into that cell. The estimated membrane time constant extracted via "peeling" the voltage transient in Figure 3B1 (Rall 1969) is shown in Figure 3B2. Increasing GJc markedly reduced the estimated τ_m. Figure 3C1,C2 shows that the larger the number of the GJs per neuron (and the larger the GJc), the lower the estimated τ_m and the lower the measured R_{in}. For example, assuming that the mean GJc is 0.1 nS, with around 30 connections per cell (purple line in Fig. 3C1,C2), both R_{in} and the effective time constant would be reduced by about 65%, compared with the values obtained when the cells are isolated (when GJc = 0 nS). Using a different approach (Amitai et al. 2002) estimated the reduction in the input resistance due to GJs to be about 50%. In this study, however, the modeled neurons were isopotential. Using the simpler case of 2 cylindrical cables connected via GJs, Supplementary Figures 6–8 provide further biophysical insights into the impact of GJs on the cable characteristics of neurons.

Based on the above results, in what follows, we outline the steps required for building a faithful active model of an electrically coupled neuronal network. Because what is typically available to researchers are biophysical measurements from single cells obtained in vitro, we start by taking these measures and build an initial (erroneous) model of an isolated cell (assuming GJc = 0) that fits the in vitro input resistance (e.g., of 160 MΩ) and the spiking characteristics of this cell. The latter used our recently developed MOO method (Druckmann et al. 2007; Hay et al. 2011 and see Materials and Methods). For L2/3 LBCs, this procedure yields an erroneous estimate for R_m of around 10 000 Ω cm^2 (see Fig. 2B for GJc = 0 nS) and a set of excitable membrane conductances that fit the in vitro spiking activity of that cell. The response of this model to a suprathreshold current step is shown in Figure 4A. The next step is to embed the modeled cell in an electrically coupled network (as in Fig. 3A, right). This will result in a marked reduction in input resistance and the effective membrane time constant of that cell (Fig. 3C1,C2) as well as a change in the firing characteristics of the modeled cell as depicted in Figure 4B. One can try to correct for the reduction in R_{in} by a corresponding increase in the injected current (Fig. 4C, red spikes). However, a better compensation for the impact of the GJs is to increase the R_m of all neurons in the network to retrieve their in vitro R_{in} (based on Fig. 2B), leaving the injected current unchanged. In fact, given this correction factor, the in vitro behavior of both the passive and the active properties of L2/3 LBCs was successfully retrieved (Fig. 4D; see Supplementary Fig. 9).

To summarize, due to the large number of GJs per L2/3 LBC, a very significant error is expected in estimating the cable properties of L2/3 LBCs (and other similar electrically coupled cells;

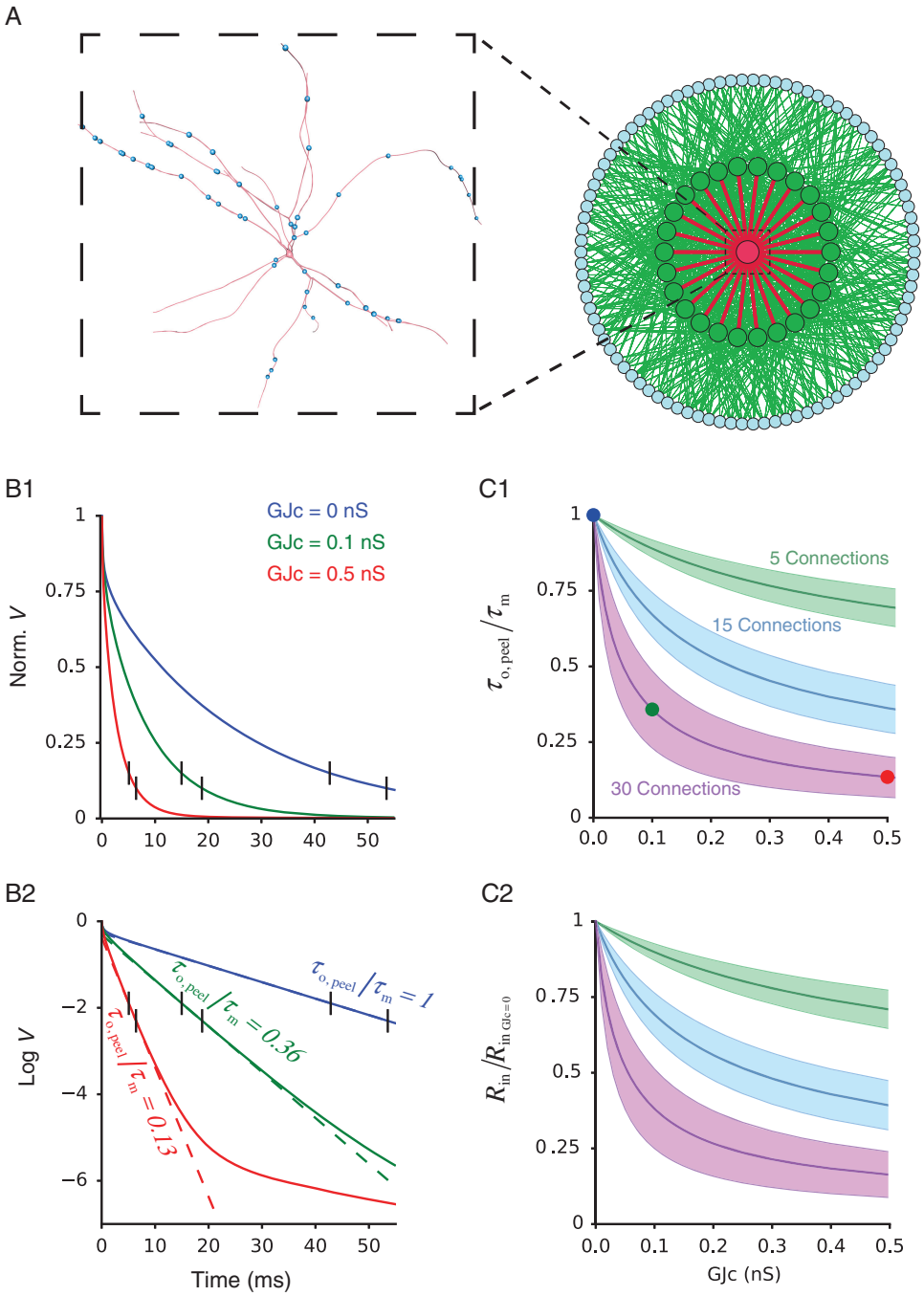

Figure 3. Distortion in L2/3 LBC cable properties due to GJs. (*A*) Right—schematic representation of the modeled L2/3 LBC neuronal network, consisting of 121 modeled L2/3 LBC neurons as in Figure 2 (an exemplar cell is shown at left, see Materials and Methods). Red—neuron of interest; green—neurons that are directly coupled with the red neuron via GJs; blue—all other neurons that are not directly connected to the red cell. Red lines depict the GJs between the green cells and the red cells (shown at left by the blue dots); green lines depict all other GJs made onto the green cells. GJs between the blue cells are not shown. (*B1*) Normalized voltage decay following a short current injection to the red cell in A, for the case of an average of 30 connections per neuron. Short vertical lines depict 85–90% decay of the initial voltage. (*B2*) "Peeling" transients for estimating the membrane time constant ($\tau_{0,peel}$) from the tail of the log of the voltage decay (peeled between 85% and 90% of the voltage decay), as typically done experimentally. Note the large underestimation of τ_m due to the GJs (green and red traces). The mean error for all neurons in estimating the membrane time constant (*C1*) and the input resistance (*C2*) as a function of GJc value is shown by the continuous line; the corresponding SD is depicted by the shaded region.

e.g., Somatostatin-to-Somatostatin, Gibson et al. 1999) extracted from in vitro measurements. In L2/3 LBCs, we predicted that due to the GJs, the input resistance and membrane time constant would both be underestimated by 2- to 4-fold. Hence, our work clearly shows that caution is mandatory when in vitro (or in vivo) measurements are used to construct cable/compartmental models of single neurons, when these neurons are intensely connected to each other via GJs. The first requirement is to correct for the impact of the GJs on the neuron's cable parameters (in other words, increase R_m accordingly); only then can the corrected neuron models be used as building blocks for models of electrically coupled networks.

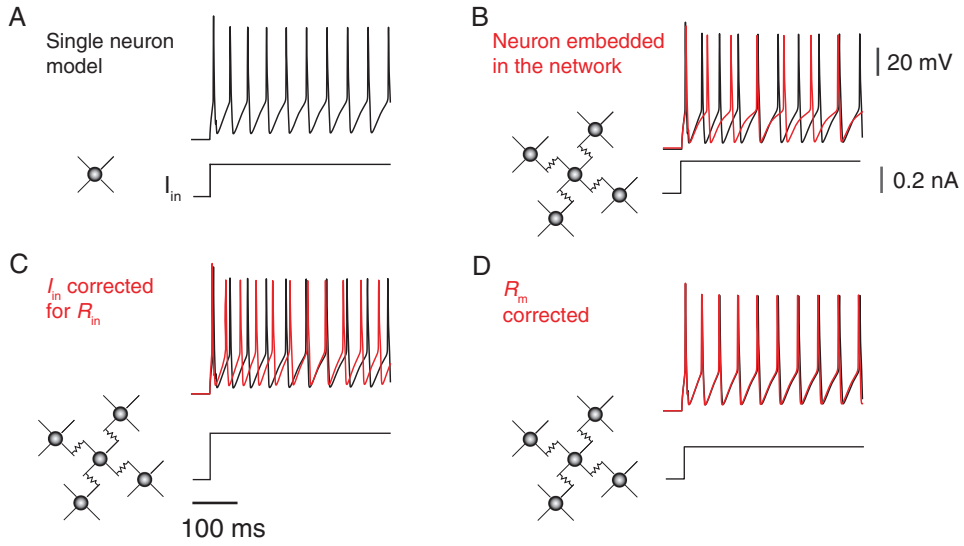

Figure 4. Effect of GJs on firing characteristics of L2/3 LBCs. (*A*) Response of a model of an isolated L2/3 LBC (cell shown in Fig. 1*A*) to suprathreshold depolarizing step current (see model parameters in Materials and Methods). (*B*) Same modeled cell as in *A*, but when the cell is embedded in a network with 30 ± 6 connections per neuron (with mean GJc = 0.11 nS). Voltage response is shown in red for the same current as in *A*. The spikes in *A* are also shown in black. (*C*) As in *B*, but compensating for the (1.4-fold) reduction in R_{in} due to the GJs by proportionally increasing the injected current. (*D*) Compensating for the effect of GJs by increasing (based on Fig. 2*B*) R_m of the modeled neurons by a factor of approximately 3 for preserving their in vitro R_{in}. This compensation successfully retrieves the spiking characteristics of the model in *A* (see also Supplementary Fig. 9).

Coincidence Detection, Improved Input Tracking, and Reduced Input Selectivity due to GJs

We explored 3 different consequences of GJs on the operation of L2/3 LBCs. In all the cases below we used a network ($n = 121$), where each neuron was connected to 30 ± 6 with 1–3 GJs per connection. As shown in Figure 3, the effective time constant of the neuron is markedly reduced when it is embedded in a network connected via GJs. This implies that postsynaptic potentials (PSPs) will decay faster in a network of L2/3 LBCs when compared with the electrically isolated case (Fig. 5*A*). In other words, the time window for synaptic integration is smaller because of the GJs.

However, this time window can be adjusted by the activation of other LBCs in the network. When a given cell is activated simultaneously with other LBCs that are directly coupled to it (Fig. 5*B*), the current sink from this cell is reduced (the network becomes more isopotential). In this condition, and depending on the number of activated cells, the PSPs are broadened, as is the time window for synaptic integration (Fig. 5*B*,*D*,*E*). Note that this broadening of the PSPs is only slight if cells that are indirectly connected to that particular cell are simultaneously activated (Fig. 5*C*).

The abovementioned result implies that an electrically coupled network behaves as a detector for coincident activation of directly coupled neurons. An L2/3 LBC might generate an output spike when it, and neurons directly connected to it, receives synchronous input (Fig. 5*E*, blue trace). The same synaptic input, when injected to that same cell and to neurons that are indirectly connected to it, will not reach threshold for spike firing (Fig. 5*E*, green trace).

We further demonstrated this "dynamic time-window effect" by activating 85 excitatory synapses per cell while increasing the number of activated cells that were directly connected to the target neuron. We examined how large the jitter could be in the activation time of these cells, while still yielding a reliably output spike at the target cell. Figure 5*F*,*G* clearly demonstrates that the temporal jitter increases steeply as the number of directly connected activated cells increases. This jitter is the time window within which the various neurons were randomly activated. For example, with 20 activated cells, the temporal jitter could be as large as 25 ms to obtain an output spike with a probability of approximately 80% (red curve in Fig. 5*F*). Hence, in electrically coupled networks, the time window for synaptic integration (and for the integration of sensory input) is adjustable, depending on both the number and configuration of the coactivated cells.

Neurons could encode rapid changes in synaptic inputs via their spike output (Ilin et al. 2013; Eyal et al. 2014; Ostojic et al. 2015). In particular, rodent pyramidal cells in the neocortex and hippocampus are capable of reliably encoding input modulations of up to 400 Hz by phase-locking their output spikes to the modulated input (Köndgen et al. 2008; Boucsein et al. 2009; Tchumatchenko et al. 2011; Ilin et al. 2013). This capability to track high-frequency modulation depends on the speed of the rising phase of the axonal spike, which is influenced by the effective time constant of the neuron (Brunel et al. 2001; Fourcaud-Trocme et al. 2003; Naundorf et al. 2005; Ilin et al. 2013; Eyal et al. 2014). Because GJs enhance the effective time constants of neurons (see above), the tracking of high-frequency modulation is expected to improve due to GJs. This is shown in Figure 6*E*.

A single neuron in the network (Fig. 6*A*) was injected with a current composed of a superposition of a small amplitude sinusoidal wave of varying frequencies and background noise (Fig. 6*B*, and see Materials and Methods). Figure 6*B* depicts the spiking response (top trace) to a DC current + noise (Fig. 6*B*, lower trace). For each sinusoidal frequency, the vector strength, *R*, which characterizes the degree of phase-locking of the neuron's APs to the sine wave, was calculated (see Materials and Methods). The phase plot of the AP measured in the axon (Eyal et al. 2014) resulting from the noisy current injection as in Figure 6*B*, for 3 values of GJc, is shown in Figure 6*C* (see corresponding colors in Fig. 6*E*). A zoom-in to the initial rising phase (box in Fig. 6*C*) is shown in Figure 6*D*. In fact, an increase in GJc results in an increase in the

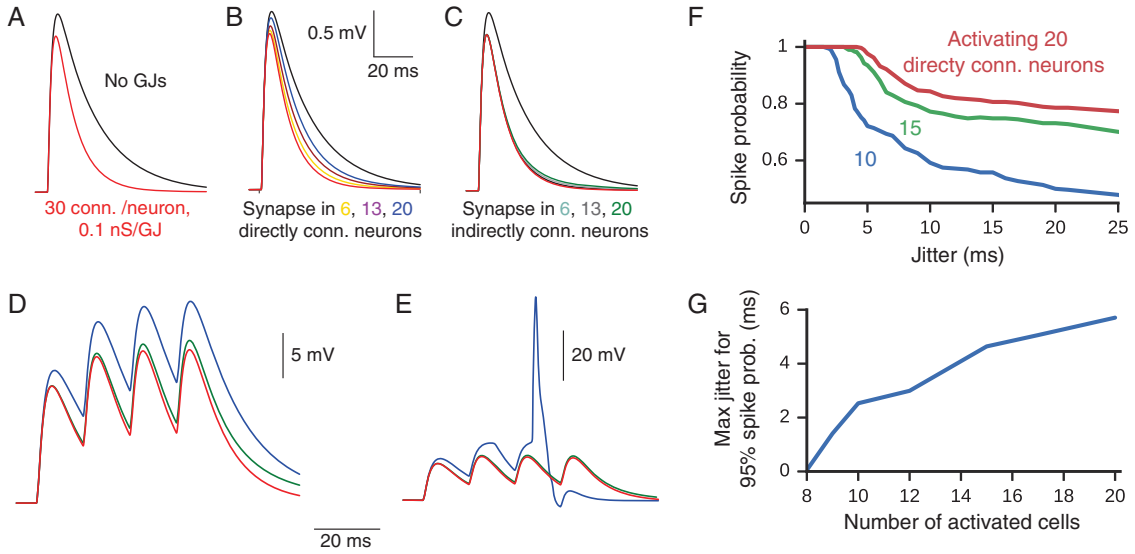

Figure 5. L2/3 LBC network as a coincidence detector. (*A*) excitatory postsynaptic potentials (EPSPs) in an isolated passive neuron with $R_m = 20\,000\ \Omega\ cm^2$ (black trace) and in the same neuron when it is embedded in an L2/3 LBC network (red trace, network consists of 30 ± 6 connections per neuron, with a mean GJc = 0.1 nS). (*B*) EPSP in the same neuron when other neurons that are directly connected to it were activated. The cases of 6, 13, and 20 simultaneously activated neurons are shown. (*C*) The corresponding cases where cells that were not directly connected to it were simultaneously activated. (*D*) A train of 4 EPSPs in the LBC of interest when 50 synapses were activated (at 71 Hz) on its dendrites (red); Green, when 20 other LBCs which were not directly connected to that cell were also activated, each by 50 excitatory dendritic synapses. Blue, when 20 neurons that were directly connected to the cell of interest were activated. (*E*) Same as in *D*, but when L2/3 LBCs consist of excitable soma (see Materials and Methods). (*F* and *G*) Dependence of the integration time window of a given neuron on the number of activated neurons that were directly connected to it (each neuron was activated with 85 excitatory synapses). Increasing the number of activated neurons was associated with an increase in the temporal jitter of the sensory input that still gives rise to a reliable spiking response.

speed of the AP rapidness (Fig. 6*D*) from 4.0 ms^{-1} in an isolated neuron (blue trace) to 4.5 ms^{-1} when GJc = 0.25 nS (green trace) resulting (Fig. 6*E*) in an increase in the cutoff frequency from 490 Hz (blue trace) to about 815 Hz (green trace). Thus, the presence of GJs between L2/3 LBCs significantly enhances their capability to track high-frequency modulations. Note that if the whole network receives simultaneous modulated input, this improvement in input tracking due to GJs is diminished (not shown).

We next examined the impact of GJs between L2/3 LBCs on visual-like sensory input. Neurons in sensory cortices are selective to specific properties of the sensory input. For example, in V1, neurons respond selectively to oriented lines presented in their visual field (Hubel and Wiesel 1959). In V1 (and also in A1 and S1), pyramidal neurons are, on average, more selective than inhibitory interneurons; that is, the tuning curve of pyramidal cells is sharper (the OSI is larger) than for nearby interneurons (Kerlin et al. 2010; Ma et al. 2010; Li et al. 2015). In addition, the linearity index (*F1/F0*, see Materials and Methods) of inhibitory neurons is smaller than that of pyramidal cells (Niell and Stryker 2008). Could GJs among inhibitory neurons affect the processing of sensory inputs by these cells?

To address this possibility, we modeled visual input impinging on the L2/3 LBC network by providing orientation selective axonal input (50 axons per cell and 5 synapses per axon). Axonal input was realized as an inhomogeneous Poisson spike train with a mean rate that was determined by the difference (in degrees) between the axon's PO and the orientation of the simulated visual input. The rate of the Poisson process was modulated at a frequency of 2 Hz, simulating a drifting grating at this frequency (see Materials and Methods). Each simulation consisted of 9 trials; each trial simulated the response to a different visual input (see Materials and Methods).

We first examined the effect of GJs on the OSI (see Materials and Methods) in the network. In the absence of GJs (GJc = 0 nS), the average OSI of the L2/3 LBC network was 0.34 (Fig. 7*A*(left), *C*). In Figure 7*B*, the firing rate of 2 cells (68, and 71, also arrows in *A*) as a function of visual orientation is shown for 3 different GJc values. Increasing the GJc decreased the orientation selectivity; this is more fully analyzed for the full network in Figure 7*C*. The mean OSI decreased from 0.34 (for GJc = 0 nS) to 0.18 (for GJc = 0.25 nS). This decrease in OSI is also depicted by the decrease in the size of the circle in Figure 7*A*. Additionally, GJs can also change the PO of the neuron (some cells, e.g., the cell denoted by asterisk in Fig. 7*A*, change color). Hence, in a network of electrically coupled neurons, as is the case of L2/3 LBCs, even a relatively small GJc may have a significant impact in shaping the OSI of the cells. Thus, the reduced OSI (and the more similar PO) found in cortical interneurons, when compared with pyramidal cells, may at least be partially due to their GJs.

We next examined the impact of GJs on the linearity index of the cells and on the phase difference among them. Figure 8*A* shows that for a selected cell (25), GJs of 0.1 nS reduce the response modulation (the *F1/F0* ratio) of that cell by about 70%. Figure 8*B* summarizes this effect for the whole population as a function of the GJc. A reduction of about 30% in response modulation could be obtained when the GJc was, on average, 0.25 nS (see Discussion). Figure 8*C* depicts the impact of GJs on the phase difference between 2 selected cells (118 and 23), whereas Figure 8*D* summarizes this effect for the whole population. On average, a marked reduction (of ~25%) in the phase difference among the cells was obtained with GJc = 0.25 nS. Figures 7 and 8 demonstrate that the "mixing" of electrically connected cells due to GJs tended to homogenize the response of the different neurons, such that their response to sensory input became more similar to each other. Note, however, that with estimated GJ values around 0.1–0.25 nS, the "mixing" of the various L2/3 LBCs was only partial. The orientation selectivity of individual cells remained intact (Fig. 7) and, although the

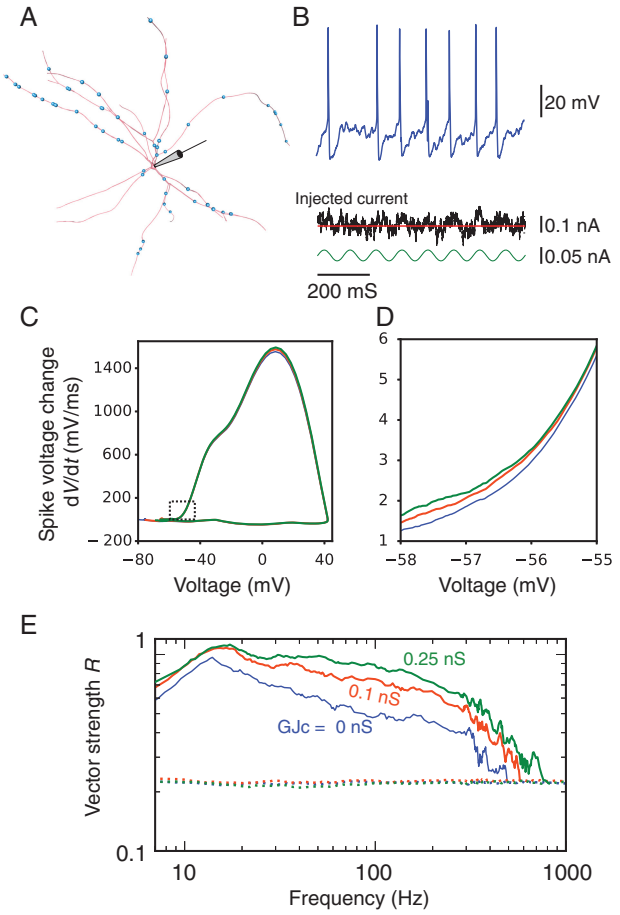

Figure 6. GJs enhance the encoding capability of the neuron. (*A*) Representation of one of the 121 modeled cells in the L2/3 LBC network. Each L2/3 LBC modeled neuron is connected to 30 ± 6 similar neurons with a mean of 2 GJs per connection (blue dots). (*B*) Spiking response (upper trace) of the neuron shown in *A*, to a noisy current injected into the cell soma (middle trace, black). The injected current was composed of a DC current (middle trace, red line), a modulated sine wave (lower trace, green line), and a noisy current (see Materials and Methods). (*C*) Phase plots of the axonal APs for 3 different GJc values (0, 0.1, and 0.25 nS). (*D*) Zoom-in to the initial part of the AP phase plots shown in *C*. Increasing GJc enhances the speed of the rising phase of the spike. (*E*) Vector strength as a function of input frequency showing the increasing capability of the modeled cell to track high-frequency input modulations with increasing GJc (value shown near the corresponding curves). The cutoff frequency is defined by the intersection between the vector strength, *R*, and the respective 95th percentile (respective dotted colored lines) obtained by computing the vector strength in 1500 random spike trains (see Materials and Methods). The cutoff frequencies were 490, 575, and 815 Hz for GJc = 0, 0.1, and 0.25 nS, respectively.

cells became more synchronized (Fig. 8*B*), they still fired at different phases.

Discussion

This study showed that GJs formed between dendrites of neocortical L2/3 LBCs significantly affect the cable properties of these cells. In particular, we estimated that due to the conductance load imposed by the electrical coupling, the input resistance, R_{in}, and membrane time constant, τ_m, of L2/3 LBCs (when decoupled from the network) are underestimated by a factor of 2–4 when measured in vitro (i.e., when they are coupled electrically). It is important to emphasize that due to the incomplete data set, we pooled data from diverse L2/3 LBC sources. Specifically, morphology and electrophysiology measurements were taken from young rats; information about the number of GJs per neuron was taken from adult cats, and the CC measurements were performed in mice. Thus, we explored a large range of parameters in terms of both the number of GJs per neuron and GJc values in order to constrain our theoretical predictions by the available biological data.

Constraining the network models of L2/3 LBCs by in vitro measurements of both R_{in} and the CC, as found between L2/3 LBCs (Figs 1 and 2), enabled us to bracket the conductance value of the GJs to range between 0.05 and 0.25 nS. This range of values holds for a variety of network configurations (Fig. 2) and is smaller than previously used (Traub et al. 2001; Hjorth et al. 2009; O'Connor et al. 2012). However, the parameters in previous modeling studies were not simultaneously constrained by both the experimental R_{in} and the CC as we did here (Fig. 2; see Supplementary Fig. 5). With GJc ranging between 0.05 and 0.25 nS, and assuming that the conductance of a single GJ channel is approximately 15 pS (Teubner et al. 2000), and that there are 140 to 360 GJ channels (connexin 36, Cx36) per GJ in L2/3 LBCs (Fukuda et al. 2006), we estimated that only 0.9–11% of the GJ channels are open. Curti et al. (2012) estimated that only 1% of the GJ channels are open. It is worth noting that the number of open GJ channels can change upon a variety of manipulations and that the GJc is adjustable (Marandykina et al. 2013; Palacios-Prado et al. 2013). This has important functional implications of our results.

Taking into account the effect of GJs on the neurons' cable properties enabled us to put forward a systematic process for building an electrically coupled network composed of these neurons. This network has the ability to faithfully replicate the in vitro (and, in principle, the in vivo) condition, in the passive measurements (Figs 2 and 3), and in the spiking activity (Fig. 4; see Supplementary Fig. 9). The impact of the network on the cable parameters of individual neurons is likely to be similar in other electrically coupled networks. Such networks have been found in many brain regions; for example, in multiple subtypes of inhibitory neocortical and hippocampal interneurons (Fukuda and Kosaka 2000; Zhang et al. 2004). There have been several experimental attempts to "get rid" of GJs. One way is to use blockers, such as carbenoxolone, but this blocker is nonspecific as it reduces the R_{in} of neurons lacking GJs (Rouach et al. 2003). Another blocker, mefloquine (which barely changes the input resistance of neurons lacking GJs), results in an increase in the R_{in} of cortical inhibitory neurons by up to 80%; however, this blocker affects only approximately 70% of the GJs (Cruikshank et al. 2004). Another approach was to use knockouts of Cx36, a neuronal GJ channel protein critical for electrical coupling between neocortical basket cells; in this case, R_{in} was increased by 35% in FS cells, when compared with the wild-type (Deans et al. 2001). However the knockout of Cx36 was found to affect the membrane properties and the size of cells in the inferior olive (De Zeeuw et al. 2003).

The impact of GJs on the spiking activity of electrically coupled neurons (Fig. 4; see Supplementary Fig. 9) results from a similar mechanism where the dendritic tree affects the spiking capabilities of the axon initial segment. In fact, both the dendritic tree and the GJs serve as a current sink (conductance load) for the excitable current underlying the AP. The larger the dendritic tree and, similarly, the larger the total GJc, the larger the conductance load on the spiking mechanism (Hay et al. 2013). The correction that we made by increasing R_m (Fig. 4; see Supplementary Fig. 9) partially compensated for the conductance load imposed by the GJs. Note that the effect of GJs was also manifested by

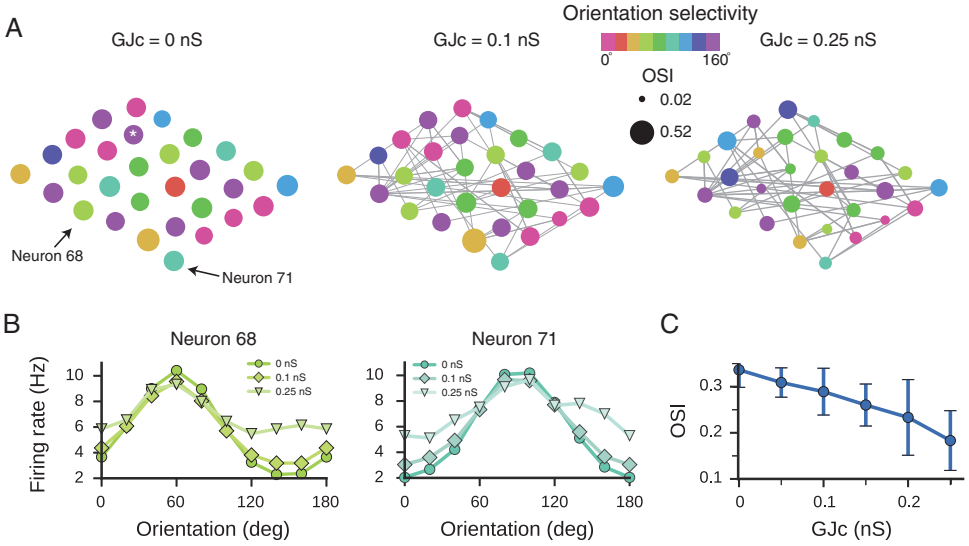

Figure 7. GJs reduce input selectivity in L2/3 LBCs network. (*A*) OSI for neurons in 3 networks that differ in their GJc values (value above each network). The PO of the modeled cells is color-coded (color scale at top) and the OSI value for each neuron is represented by the size of the circle (2 exemplar black circles at top). Only part of the modeled network is shown with only 10% of the GJs, which are depicted by the lines connecting the neurons. Note the decrease in the size of the circles (decreased OSI) with increasing GJc and also the change in PO (change in color) of some cells (e.g., the cell marked by asterisk). (*B*) Tuning curves of 2 exemplar neurons (68 and 71), for 3 values of GJc. (*C*) The mean OSI + SD for the whole network consisting of 121 L2/3 LBCs as a function of GJc; the larger the GJc value, the lower the OSI. In all cases, the average firing rate of the network was adjusted to 10 Hz (see Materials and Methods).

enhancing the rising phase of the AP (Fig. 6C) which affects the tracking capability of the axonal spikes (see below).

Once we established reliable models for individual L2/3 LBCs, we were in a position to examine a few key functional aspects of GJs in L2/3 LBC networks. We showed that synaptic inputs impinging on individual neurons decay faster due to the GJs, and thus shorten the integration time window. This effect could be modulated by the coactivation of directly connected neurons in the network. In fact, we showed that the effective integration time window increases (by several fold) when more neurons are activated simultaneously (Fig. 5). This implies that a presynaptic excitatory neuron that synapses onto several interneurons is more likely to activate these interneurons if they are directly coupled with each other via GJs (Fig. 5E). A recent study demonstrated that interneurons that are electrically coupled are more likely to have a common presynaptic excitatory input (Otsuka and Kawaguchi 2013). We further demonstrated this "dynamic time-window effect" by showing that the temporal jitter of a sensory-like input, which generated a reliable spiking response, depended to a great extent on the number of the activated cells and on the identity of the cells that were activated (Fig. 5F,G).

Another effect of the reduction in the effective (system) time constant due to GJs was the increase in speed (upstroke) of spike initiation (Fig. 6). This improved the capability of individual L2/3 LBCs to track high-frequency input modulations via their spike output (Fourcaud-Trocme et al. 2003; Ilin et al. 2013; Eyal et al. 2014). For individual L2/3 LBCs, a 2-fold increase in the cutoff frequency (from 490 to 815 Hz) was found when the GJc was increased from 0 to 0.25 nS (Fig. 6). However, if the whole electrically coupled network received simultaneously modulated input (because the GJ-induced conductance load was effectively reduced), the improvement in the tracking capability of individual cells was reduced (not shown). Note that this improvement of inhibitory interneurons in tracking rapid changes in synaptic input goes hand in hand with the increase in FR of

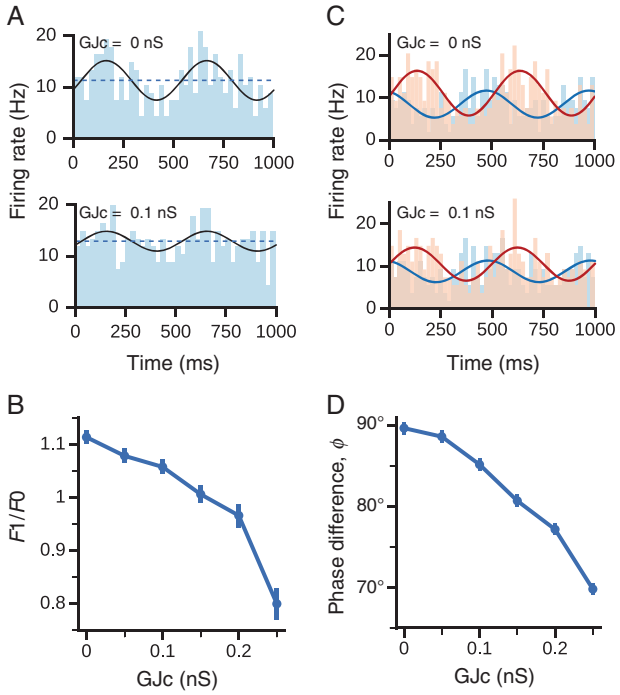

Figure 8. Influence of GJs on visual-like sensory input. (*A*) Spiking activity of a neuron in response to an oscillating axonal input, the linearity index of the cell decreased from 1.8 to 0.55 when GJs were added to the network (at 0.1 nS, lower graph). The decrease in linearity due to GJs is manifested by the lower amplitude of the sine wave, which was computed as the best 2 Hz sinusoidal fit (continuous line) to the spike histogram (blue histogram). (*B*) Mean linearity as a function of GJc. (*C*) Spiking histogram for 2 different cells without GJs (top) and with GJc = 0.1 nS (bottom). The phase difference between the cells decreases as the conductance of the GJs increases. (*D*) Mean phase difference across all cell pairs in the network (vertical lines in *B* and *D* represent standard error of the mean).

these cells due to the GJs (see Supplementary Fig. 9D, green dots). Improved tracking capability has been shown to be correlated with the firing frequency of the cell (Fourcaud-Trocme et al. 2003).

We further examined (Fig. 7) the impact of GJs on input selectivity of L2/3 LBCs, considering the case of a "salt and pepper" organization as found in the visual (and auditory) system of rodents, where adjacent cells have mixed receptive fields (Ohki and Reid 2007; Rothschild et al. 2010). In this scenario, GJs among inhibitory neurons reduced the cells' orientation selectivity (the receptive field was broadened), when compared with cells lacking GJs. Furthermore, the receptive fields of the inhibitory interneurons became more similar to each other as a result of the GJs. This is consistent with a recent finding that the orientation selectivity of interneurons is lower than that of nearby excitatory cells (Ma et al. 2010; Li et al. 2015). We also found (Fig. 8) that in the presence of GJs, both the linearity index and the phase difference among the electrically coupled cells decreased. Elsewhere, it was shown experimentally that the linearity index in inhibitory neurons is smaller than that of pyramidal cells (Niell and Stryker 2008). Our results also support the recent findings that inhibitory neurons are more binocular than excitatory neurons (Kameyama et al. 2010; Scholl et al. 2015) and that the disparity selectivity in PV^+ interneurons is weaker than in PV^- neurons (Scholl et al. 2015). We propose to experimentally test our predictions regarding the effect of GJs on the processing of visual input in Cx36 knockout animals. We predict that, in this case, the interneurons will be more highly tuned to specific features of the visual input. Clearly, a full theoretical exploration of the effect of GJs on the processing of sensory input requires the addition of recurrent chemical synapses (inhibitory and excitatory) impinging on L2/3 LBCs.

Having realistic models of electrically coupled networks will enable us to further explore the impact of electrical synapses among groups of interneurons on the global dynamics of large-scale neuronal circuits. How does global network synchronization emerge from assemblies of electrically coupled interneurons? What characterizes the interaction between electrically coupled subnetworks (e.g., networks of LBCs connected to Martinotti cell networks)? How is the receptive field of excitatory neurons shaped by the different electrically coupled inhibitory subnetworks? These and related questions could be investigated through the construction of increasingly more faithful in silico models of neural microcircuits (Egger et al. 2014; Markram et al. 2015; Reimann et al. 2015).

Supplementary Material

Supplementary material can be found at http://www.cercor.oxfordjournals.org/.

Funding

This work was supported by funding from the EPFL to the Laboratory of Neural Microcircuitry (LNMC), funding from the ETH Domain for the Blue Brain Project (BBP), and by funding to the Human Brain Project from the European Union Seventh Framework Program (FP7/2007-2013) under grant agreement no. 604102. Additional funding came from The Gatsby Charitable Foundation, and an EPFL-Hebrew University Collaborative Grant. The BlueBrain IV BlueGene/Q system is financed by ETH Board Funding to the Blue Brain Project as a National Research Infrastructure and hosted at the Swiss National Supercomputing Center (CSCS). Funding to pay the Open Access publication charges for this article was provided by the Human Brain Project from the European Union Seventh Frame-work Program (FP7/2007-2013) under grant agreement no. 604102.

Notes

We thank Juan Hernando for helping with the visualization in this work and to Guy Eyal and Yoav Tal for their useful comments during this project. *Conflict of Interest*: None declared.

References

Alcami P, Marty A. 2013. Estimating functional connectivity in an electrically coupled interneuron network. Proc Natl Acad Sci USA. 110:E4798–E4807.

Amitai Y, Gibson JR, Beierlein M, Patrick SL, Ho AM, Connors BW, Golomb D. 2002. The spatial dimensions of electrically coupled networks of interneurons in the neocortex. J Neurosci. 22:4142–4152.

Anastasiades PG, Marques-Smith A, Lyngholm D, Lickiss T, Raffiq S, Kätzel D, Miesenböck G, Butt SJB. 2016. GABAergic interneurons form transient layer-specific circuits in early postnatal neocortex. Nat Commun. 7:10584.

Angulo MC, Rossier J, Audinat E. 1999. Postsynaptic glutamate receptors and integrative properties of fast-spiking interneurons in the rat neocortex. J Neurophysiol. 82:1295–1302.

Avermann M, Tomm C, Mateo C, Gerstner W, Petersen CCH. 2012. Microcircuits of excitatory and inhibitory neurons in layer 2/3 of mouse barrel cortex. J Neurophysiol. 107:3116–3134.

Bennett MVL. 1977. Electrical transmission: a functional analysis and comparison to chemical transmission. In: Kandel ER, editor. Handbook of physiology, Sec I, The nervous system, Vol 1, Cellular biology of neurons, Pt 1. Bethesda, MD: American Physiological Society. p. 357–416.

Berens P. 2009. CircStat: a MATLAB toolbox for circular statistics. J Stat Softw. 31:1–21.

Boucsein C, Tetzlaff T, Meier R, Aertsen A, Naundorf B. 2009. Dynamical response properties of neocortical neuron ensembles: multiplicative versus additive noise. J Neurosci. 29:1006–1010.

Brunel N, Chance FS, Fourcaud N, Abbott LF. 2001. Effects of synaptic noise and filtering on the frequency response of spiking neurons. Phys Rev Lett. 86:2186–2189.

Buhl DL, Harris KD, Hormuzdi SG, Monyer H, Buzsáki G. 2003. Selective impairment of hippocampal gamma oscillations in connexin-36 knock-out mouse in vivo. J Neurosci. 23:1013–1018.

Carnevale NT, Hines ML. 2006. The NEURON Book. Cambridge, UK: Cambridge University Press.

Chow CC, Kopell N. 2000. Dynamics of spiking neurons with electrical coupling. Neural Comput. 12:1643–1678.

Cruikshank SJ, Hopperstad M, Younger M, Connors BW, Spray DC, Srinivas M. 2004. Potent block of Cx36 and Cx50 gap junction channels by mefloquine. Proc Natl Acad Sci USA. 101:12364–12369.

Curti S, Hoge G, Nagy JI, Pereda AE. 2012. Synergy between electrical coupling and membrane properties promotes strong synchronization of neurons of the mesencephalic trigeminal nucleus. J Neurosci. 32:4341–4359.

Deans MR, Gibson JR, Sellitto C, Connors BW, Paul DL. 2001. Synchronous activity of inhibitory networks in neocortex requires electrical synapses containing connexin36. Neuron. 31:477–485.

Dere E, Zlomuzica A, Binder S. 2012. Gap junctions in the brain: physiological and pathological roles, gap junctions in the brain. London: Academic Press.

Devor A, Yarom Y. 2002. Electrotonic coupling in the inferior olivary nucleus revealed by simultaneous double patch recordings. J Neurophysiol. 87:3048–3058.

De Zeeuw CI, Chorev E, Devor A, Manor Y, Van Der Giessen RS, De Jeu MT, Hoogenraad CC, Bijman J, Ruigrok TJH, French P, et al. 2003. Deformation of network connectivity in the inferior olive of connexin 36-deficient mice is compensated by morphological and electrophysiological changes at the single neuron level. J Neurosci. 23:4700–4711.

Druckmann S, Banitt Y, Gidon A, Schürmann F, Markram H, Segev I. 2007. A novel multiple objective optimization framework for constraining conductance-based neuron models by experimental data. Front Neurosci. 1:7–18.

Druckmann S, Hill S, Schürmann F, Markram H, Segev I. 2013. A hierarchical structure of cortical interneuron electrical diversity revealed by automated statistical analysis. Cereb Cortex. 23:2994–3006.

Egger R, Dercksen VJ, Udvary D, Hege H-C, Oberlaender M. 2014. Generation of dense statistical connectomes from sparse morphological data. Front Neuroanat. 8:129.

Eyal G, Mansvelder HD, de Kock CPJ, Segev I. 2014. Dendrites impact the encoding capabilities of the axon. J Neurosci. 34:8063–8071.

Fourcaud-Trocme N, Hansel D, van Vreeswijk C, Brunel N. 2003. How spike generation mechanisms determine the neuronal response to fluctuating inputs. J Neurosci. 23:11628–11640.

Fukuda T, Kosaka T. 2000. Gap junctions linking the dendritic network of GABAergic interneurons in the hippocampus. J Neurosci. 20:1519–1528.

Fukuda T, Kosaka T, Singer W, Galuske RAW. 2006. Gap junctions among dendrites of cortical GABAergic neurons establish a dense and widespread intercolumnar network. J Neurosci. 26:3434–3443.

Galarreta M, Hestrin S. 2002. Electrical and chemical synapses among parvalbumin fast-spiking GABAergic interneurons in adult mouse neocortex. Proc Natl Acad Sci USA. 99: 12438–12443.

Galarreta M, Hestrin S. 1999. A network of fast-spiking cells in the neocortex connected by electrical synapses. Nature. 402: 72–75.

Gentet LJ, Avermann M, Matyas F, Staiger JF, Petersen CCH. 2010. Membrane potential dynamics of GABAergic neurons in the barrel cortex of behaving mice. Neuron. 65:422–435.

Gibson JR, Beierlein M, Connors BW. 2005. Functional properties of electrical synapses between inhibitory interneurons of neocortical layer 4. J Neurophysiol. 93:467–480.

Gibson JR, Beierlein M, Connors BW. 1999. Two networks of electrically coupled inhibitory neurons in neocortex. Nature. 402:75–79.

Goodenough DA, Paul DL. 2009. Gap junctions. Cold Spring Harb Perspect Biol. 1:a002576.

Gupta A. 2000. Organizing principles for a diversity of GABAergic interneurons and synapses in the neocortex. Science. 287:273–278.

Hay E, Hill S, Schürmann F, Markram H, Segev I. 2011. Models of neocortical layer 5b pyramidal cells capturing a wide range of dendritic and perisomatic active properties. PLoS Comput Biol. 7:e1002107.

Hay E, Schürmann F, Markram H, Segev I. 2013. Preserving axosomatic spiking features despite diverse dendritic morphology. J Neurophysiol. 109:2972–2981.

Hjorth J, Blackwell KT, Kotaleski JH. 2009. Gap junctions between striatal fast-spiking interneurons regulate spiking activity and synchronization as a function of cortical activity. J Neurosci. 29:5276–5286.

Hochstein S, Shapley RM. 1976. Quantitative analysis of retinal ganglion cell classifications. J Physiol. 262:237–264.

Hu H, Agmon A. 2015. Properties of precise firing synchrony between synaptically coupled cortical interneurons depend on their mode of coupling. J Neurophysiol. 114:624–637.

Hubel DH, Wiesel TN. 1959. Receptive fields of single neurones in the cat's striate cortex. J Physiol. 148:574–591.

Ilin V, Malyshev A, Wolf F, Volgushev M. 2013. Fast computations in cortical ensembles require rapid initiation of action potentials. J Neurosci. 33:2281–2292.

Jeyabalaratnam J, Bharmauria V, Bachatene L, Cattan S, Angers A, Molotchnikoff S. 2013. Adaptation shifts preferred orientation of tuning curve in the mouse visual cortex. PLoS ONE. 8: e64294.

Kameyama K, Sohya K, Ebina T, Fukuda A, Yanagawa Y, Tsumoto T. 2010. Difference in binocularity and ocular dominance plasticity between GABAergic and excitatory cortical neurons. J Neurosci. 30:1551–1559.

Kerlin AM, Andermann ML, Berezovskii VK, Reid RC. 2010. Broadly tuned response properties of diverse inhibitory neuron subtypes in mouse visual cortex. Neuron. 67:858–871.

Köndgen H, Geisler C, Fusi S, Wang X-J, Lüscher H-R, Giugliano M. 2008. The dynamical response properties of neocortical neurons to temporally modulated noisy inputs in vitro. Cereb Cortex. 18:2086–2097.

Lewis TJ, Rinzel J. 2003. Dynamics of spiking neurons connected by both inhibitory and electrical coupling. J Comput Neurosci. 14:283–309.

Li L-Y, Xiong XR, Ibrahim LA, Yuan W, Tao HW, Zhang LI. 2015. Differential receptive field properties of parvalbumin and somatostatin inhibitory neurons in mouse auditory cortex. Cereb Cortex. 25:1782–1791.

Ma W-P, Liu B-H, Li Y-T, Huang ZJ, Zhang LI, Tao HW. 2010. Visual representations by cortical somatostatin inhibitory neurons—selective but with weak and delayed responses. J Neurosci. 30:14371–14379.

Manor Y, Rinzel J, Segev I, Yarom Y. 1997. Low-amplitude oscillations in the inferior olive: a model based on electrical coupling of neurons with heterogeneous channel densities. J Neurophysiol. 77:2736–2752.

Marandykina A, Palacios-Prado N, Rimkut? L, Skeberdis VA, Bukauskas FF. 2013. Regulation of connexin36 gap junction channels by n-alkanols and arachidonic acid. J Physiol. 591:2087–2101.

Markram H, Muller E, Ramaswamy S, Reimann MW, Abdellah M, Sanchez CA, Ailamaki A, Alonso-Nanclares L, Antille N, Arsever S, et al. 2015. Reconstruction and simulation of neocortical microcircuitry. Cell. 163:456–492.

Mathy A, Clark BA, Häusser M. 2014. Synaptically induced long-term modulation of electrical coupling in the inferior olive. Neuron. 81:1290–1296.

Meyer AH, Katona I, Blatow M, Rozov A, Monyer H. 2002. In vivo labeling of parvalbumin-positive interneurons and analysis of electrical coupling in identified neurons. J Neurosci. 22:7055–7064.

Naundorf B, Geisel T, Wolf F. 2005. Action potential onset dynamics and the response speed of neuronal populations. J Comput Neurosci. 18:297–309.

Naundorf B, Wolf F, Volgushev M. 2006. Unique features of action potential initiation in cortical neurons. Nature. 440: 1060–1063.

Niell CM, Stryker MP. 2008. Highly selective receptive fields in mouse visual cortex. J Neurosci. 28:7520–7536.
Niell CM, Stryker MP. 2010. Modulation of visual responses by behavioral state in mouse visual cortex. Neuron. 65:472–479.
O'Connor S, Angelo K, Jacob TJC. 2012. Burst firing versus synchrony in a gap junction connected olfactory bulb mitral cell network model. Front Comput Neurosci. 6:75.
Ohki K, Reid RC. 2007. Specificity and randomness in the visual cortex. Curr Opin Neurobiol. 17:401–407.
Ostojic S, Szapiro G, Schwartz E, Barbour B, Brunel N, Hakim V. 2015. Neuronal morphology generates high-frequency firing resonance. J Neurosci. 35:7056–7068.
Otsuka T, Kawaguchi Y. 2013. Common excitatory synaptic inputs to electrically connected cortical fast-spiking cell networks. J Neurophysiol. 110:795–806.
Palacios-Prado N, Hoge G, Marandykina A, Rimkute L, Chapuis S, Paulauskas N, Skeberdis VA, O'Brien J, Pereda AE, Bennett MVL, et al. 2013. Intracellular magnesium-dependent modulation of gap junction channels formed by neuronal connexin36. J Neurosci. 33:4741–4753.
Paré D, Shink E, Gaudreau H, Destexhe A, Lang EJ. 1998. Impact of spontaneous synaptic activity on the resting properties of cat neocortical pyramidal neurons in vivo. J Neurophysiol. 79:1450–1460.
Pereda AE. 2014. Electrical synapses and their functional interactions with chemical synapses. Nat Rev Neurosci. 15:250–263.
Pfeuty B, Golomb D, Mato G, Hansel D. 2007. Inhibition potentiates the synchronizing action of electrical synapses. Front Comput Neurosci. 1:8.
Pfeuty B, Mato G, Golomb D, Hansel D. 2003. Electrical synapses and synchrony: the role of intrinsic currents. J Neurosci. 23:6280–6294.
Prinz AA, Fromherz P. 2003. Effect of neuritic cables on conductance estimates for remote electrical synapses. J Neurophysiol. 89:2215–2224.
Rall W. 1959. Branching dendritic trees and motoneuron membrane resistivity. Exp Neurol. 1:491–527.
Rall W. 1977. Core conduction theory and cable properties of neurons. Handb Physiol Nerv Syst. I:36–97.
Rall W. 1969. Time constants and electrotonic length of membrane cylinders and neurons. Biophys J. 9:1483–1508.
Rash JE, Curti S, Vanderpool KG, Kamasawa N, Nannapaneni S, Palacios-Prado N, Flores CE, Yasumura T, O'Brien J, Lynn BD, et al. 2013. Molecular and functional asymmetry at a vertebrate electrical synapse. Neuron. 79:957–969.
Rauch A, La Camera G, Luscher H-R, Senn W, Fusi S. 2003. Neocortical pyramidal cells respond as integrate-and-fire neurons to in vivo-like input currents. J Neurophysiol. 90: 1598–1612.
Reimann MW, King JG, Muller EB, Ramaswamy S, Markram H. 2015. An algorithm to predict the connectome of neural microcircuits. Front Comput Neurosci. 9:120.
Rieubland S, Roth A, Häusser M. 2014. Structured connectivity in cerebellar inhibitory networks. Neuron. 81:913–929.
Rothschild G, Nelken I, Mizrahi A. 2010. Functional organization and population dynamics in the mouse primary auditory cortex. Nat Neurosci. 13:353–360.
Rouach N, Segal M, Koulakoff A, Giaume C, Avignone E. 2003. Carbenoxolone blockade of neuronal network activity in culture is not mediated by an action on gap junctions. J Physiol. 553:729–745.
Russo G, Nieus TR, Maggi S, Taverna S. 2013. Dynamics of action potential firing in electrically connected striatal fast-spiking interneurons. Front Cell Neurosci. 7:209.
Saraga F, Zhang XL, Zhang L, Carlen PL, Skinner FK. 2006. Exploring gap junction location and density in electrically coupled hippocampal oriens interneurons. Neurocomputing. 69:1048–1052.
Schmitz D, Schuchmann S, Fisahn A, Draguhn A, Buhl EH, Petrasch-Parwez E, Dermietzel R, Heinemann U, Traub RD. 2001. Axo-axonal coupling: a novel mechanism for ultrafast neuronal communication. Neuron. 31:831–840.
Scholl B, Pattadkal JJ, Dilly GA, Priebe NJ, Zemelman BV. 2015. Local integration accounts for weak selectivity of mouse neocortical parvalbumin interneurons. Neuron. 87:424–436.
Simon A, Oláh S, Molnár G, Szabadics J, Tamás G. 2005. Gap-junctional coupling between neurogliaform cells and various interneuron types in the neocortex. J Neurosci. 25:6278–6285.
Simon A, Traub RD, Vladimirov N, Jenkins A, Nicholson C, Whittaker RG, Schofield I, Clowry GJ, Cunningham MO, Whittington MA. 2014. Gap junction networks can generate both ripple-like and fast ripple-like oscillations. Eur J Neurosci. 39:46–60.
Swindale NV. 1998. Orientation tuning curves: empirical description and estimation of parameters. Biol Cybern. 78:45–56.
Tamás G, Buhl EH, Lörincz A, Somogyi P. 2000. Proximally targeted GABAergic synapses and gap junctions synchronize cortical interneurons. Nat Neurosci. 3:366–371.
Tchumatchenko T, Malyshev A, Wolf F, Volgushev M. 2011. Ultrafast population encoding by cortical neurons. J Neurosci. 31:12171–12179.
Teubner B, Degen J, Söhl G, Güldenagel M, Bukauskas FF, Trexler EB, Verselis VK, De Zeeuw CI, Lee CG, Kozak CA, et al. 2000. Functional expression of the murine connexin 36 gene coding for a neuron-specific gap junctional protein. J Membr Biol. 176:249–262.
Torben-Nielsen B, Segev I, Yarom Y. 2012. The generation of phase differences and frequency changes in a network model of inferior olive subthreshold oscillations. PLoS Comput Biol. 8:e1002580.
Traub RD, Draguhn A, Whittington MA, Baldeweg T, Bibbig A, Buhl EH, Schmitz D. 2002. Axonal gap junctions between principal neurons: a novel source of network oscillations, and perhaps epileptogenesis. Rev Neurosci. 13:1–30.
Traub RD, Kopell N, Bibbig A, Buhl EH, LeBeau FEN, Whittington MA. 2001. Gap junctions between interneuron dendrites can enhance synchrony of gamma oscillations in distributed networks. J Neurosci. 21:9478–9486.
Vervaeke K, Lorincz A, Gleeson P, Farinella M, Nusser Z, Silver RA. 2010. Rapid desynchronization of an electrically coupled interneuron network with sparse excitatory synaptic input. Neuron. 67:435–451.
Vladimirov N, Tu Y, Traub RD. 2013. Synaptic gating at axonal branches, and sharp-wave ripples with replay: a simulation study. Eur J Neurosci. 38:3435–3447.
Wang Y, Gupta A, Toledo-Rodriguez M, Wu CZ, Markram H. 2002. Anatomical, physiological, molecular and circuit properties of nest basket cells in the developing somatosensory cortex. Cereb Cortex. 12:395–410.
Xiang Z, Huguenard JR, Prince DA. 1998. $GABA_A$ receptor-mediated currents in interneurons and pyramidal cells of rat visual cortex. J Physiol. 506:715–730.
Zhang X-L, Zhang L, Carlen PL. 2004. Electrotonic coupling between stratum oriens interneurones in the intact in vitro mouse juvenile hippocampus. J Physiol. 558:825–839.
Zhou F, Hablitz J. 1996. Postnatal development of membrane properties of layer I neurons in rat neocortex. J Neurosci. 16:1131–1139.